Estuarine, Coastal and Shelf Science 331 (2026) 109719

Contents lists available at ScienceDirect

Estuarine, Coastal and Shelf Science

journal homepage: www.elsevier.com/locate/ecss

Machine learning-based detection of mangrove dynamics in a subtropical bay: reasons and outcomes

Xiaowen Xie [a,b], Zhijun Dai [a,b,c,*], Riming Wang [a,b,**], Tianliang Wu [a,b,d], Baoqing Hu [a,b], Xixing Liang [a,b,c,d]

[a] Guangxi Key Laboratory of Marine Environmental Change and Disaster in Beibu Gulf, Beibu Gulf University (Qinzhou), 535011, China

[b] Key Laboratory of Environment Change and Resources Use in Beibu Gulf, Ministry of Education, Nanning Normal University, Nanning, 530001, China

[c] State Key Laboratory of Estuarine and Coastal Research, East China Normal University, Shanghai, 200062, China

[d] Guangxi Academy of Oceanography, Nanning, 530022, China

ARTICLE INFO

Keywords:
Dynamic changes
Mangrove forests
Hydro-sediment
Anthropogenic activities
Sea level rise
Machine learning

ABSTRACT

Mangrove forests constitute one of the most carbon-dense ecosystems in tropical and subtropical intertidal zones, providing significant ecological and economic benefits worldwide. Nevertheless, these vital ecosystems have experienced substantial degradation in recent decades, primarily attributable to escalating anthropogenic pressures and rising sea levels. Here, this study employed remote sensing imagery (1987–2023) and machine learning to examine mangrove forest dynamics in Fangcheng Bay (FCB), a subtropical bay in China's Beibu Gulf. Our analysis demonstrated a remarkable 182.38 % expansion in FCB's mangrove coverage over the 36-year period (1987–2023), with total area increasing from 233.19 ha to 658.49 ha. The West Bay (WB) and East Bay (EB) exhibited respective increases of 52.98 % and 274.47 %. Meanwhile, landward mangroves declined while seaward expansion occurred at an average shoreline progression rate of 1.28 m/yr. Furtherly, our analysis indicates that neither sea level rise nor estuarine declining suspended sediment concentration significantly influenced mangrove expansion. Tidal current-driven sediment deposition created optimal growth conditions by continuously replenishing mangrove tidal flats. These findings elucidate the drivers and patterns of FCB's mangrove dynamics amid rapid urbanization, offering critical implications for global mangrove conservation in comparable bay systems.

1. Introduction

Mangrove forests in the intertidal zones of tropical and subtropical regions are among the most crucial ecosystems on earth (Donato et al., 2011; Morrissette et al., 2023). They play a pivotal role in nutrient accumulation, water purification, shoreline protection, wave attenuation, and providing habitats for biodiversity (Alongi, 2002; Hogarth, 2015; Raju and Arockiasamy, 2022; Su et al., 2021; Hu et al., 2014, 2025). Meanwhile, mangrove ecosystems, as a crucial component of blue carbon, store approximately five times more soil carbon than terrestrial ecosystems (Gao et al., 2016; Donato et al., 2011; Chen et al., 2021). Mangrove ecosystems rank among the most critically threatened coastal habitats worldwide (Kuenzer et al., 2011), with global coverage declining dramatically from 187,940 km^2 in 1980 to 145,068 km^2 in 2020 (FAO, 2007; Jia et al., 2023). This dramatic decline of approximately 23 % in global mangrove coverage over four decades has propelled mangrove ecosystem dynamics and conservation to the forefront of international environmental priorities (FAO, 2007; Dai et al., 2024).

The dynamic changes of mangroves are influenced by a complex interplay of environmental and anthropogenic factors (Thomas et al., 2017). A substantial body of research has identified sea-level rise (SLR) as a significant potential threat to intertidal mangroves, which may force these ecosystems to undergo landward retreat (Gilman et al., 2007; Kirwan and Megonigal, 2013; Krauss et al., 2014; Mafi-Gholami et al., 2020). According to the Food and Agriculture Organization (FAO, 2023), natural factors, including SLR, could contribute to 26 % of the global mangrove forest loss between 2000 and 2020. Projections suggest that by 2050, SLR could result in the loss of up to 23,672 km^2 of

This article is part of a special issue entitled: ECSA60 YECSS published in Estuarine, Coastal and Shelf Science.

* Corresponding author. State Key Laboratory of Estuarine and Coastal Research, East China Normal University, Shanghai, 200062, China.
** Corresponding author. Guangxi Key Laboratory of Marine Environmental Change and Disaster in Beibu Gulf, Beibu Gulf University (Qinzhou), 535011, China.
E-mail addresses: zjdai@sklec.ecnu.edu.cn (Z. Dai), wangriming@bbgu.edu.cn (R. Wang).

https://doi.org/10.1016/j.ecss.2026.109719
Received 13 May 2025; Received in revised form 15 December 2025; Accepted 16 January 2026
Available online 19 January 2026

mangrove habitats worldwide (IUCN, 2024).

However, emerging evidence challenges this paradigm, demonstrating that SLR does not universally lead to mangrove disappearance (Long et al., 2022; Wu et al., 2025a). In estuarine systems where sediment accretion rates exceed the rate of SLR, mangroves have been observed to expand seaward (Long et al., 2022; Xiong et al., 2024). This phenomenon is particularly evident in the Nanliu River Delta and Red River Delta, where ongoing seaward expansion of mangrove forests has been documented (Long et al., 2021, 2022). The vulnerability of mangroves to SLR appears to be highly dependent on local hydrogeomorphic conditions, including sediment supply, tidal regime, and coastal geomorphology (Lovelock et al., 2015; Berger et al., 2008; Krauss et al., 2014). These findings underscore the importance of site-specific assessments when evaluating SLR impacts on mangrove ecosystems.

Meanwhile, human activities have caused irreversible loss of mangroves (Friess et al., 2019; Chen et al., 2009). Between 2000 and 2016, human activities were responsible for 62 % of the global mangrove loss (Goldberg et al., 2020; Simard et al., 2008). The expansion of aquaculture ponds and agricultural land was the main contributor to mangrove loss (Bunting et al., 2022). In Vietnam, aquaculture ponds and farmland expansion were responsible for 68.2 % of mangrove loss from 2010 to 2019 (Tinh et al., 2022). In Chilaw Lagoon, between 1973 and 2020, the expansion of aquaculture ponds accounted for 92 % of mangrove loss (Ofori et al., 2023). In Myanmar, 293,035 ha of mangroves were lost due to agricultural expansion between 1975 and 2005 (Giri et al., 2008). Furthermore, urbanization was also one of the significant factors in the loss of mangroves (Goldberg et al., 2020). Between 2000 and 2016, urban development resulted in the loss of 96 ± 15 km^2 of mangroves worldwide (Richards and Friess, 2016). In China, urban construction induced the loss of 942 ha of mangroves between 1985 and 2018 (Zheng and Takeuchi, 2020). Therefore, understanding the complex factors driving mangrove forest dynamics is crucial for the conservation and management of these ecosystems.

Mangroves predominantly inhabit intertidal zones within estuarine, deltaic, and bay environments, where their spatial distribution and growth dynamics are governed by complex hydrodynamic processes, including riverine discharge, wave action, and tidal regimes (Cannon et al., 2020; Crase et al., 2013). River-derived sediment supply plays a fundamental role in creating suitable substrates for mangrove colonization and expansion (Swales et al., 2019). A notable example is the Amazon River estuary, where high sediment loads have facilitated extensive mangrove progradation (Nascimento et al., 2013). Conversely, anthropogenic interventions such as upstream dam construction have significantly reduced sediment delivery to the Mekong Delta, resulting in widespread mangrove erosion (Besset et al., 2019).

Wave energy represents another critical control on mangrove stability. High-energy wave conditions have driven substantial mangrove retreat in the Fly River Delta and Irrawaddy Delta (Wu et al., 2025b; Xiong et al., 2024). Additionally, the interplay between tidal currents and wave action influences sediment redistribution, which in turn affects mangrove development (Long et al., 2021). For instance, in the Indus Delta, tidal currents transport wave-resuspended sediments into mangrove tidal creeks, enhancing sediment accretion and facilitating mangrove expansion (Zhou et al., 2024).

In contrast, semi-enclosed bays exhibit distinct hydrodynamic regimes characterized by topographic constraints and attenuated wave energy, often resulting in tide-dominated sedimentary environments (Torres-Córdoba et al., 2025; Ryu, 2003). These unique hydrodynamic conditions may lead to divergent mangrove evolutionary trajectories compared to open-coast estuaries and deltas. However, while numerous studies have examined mangrove dynamics in wave and river-dominated settings, research on tide-dominated semi-enclosed bays remains limited. Fangcheng Bay (FCB), a subtropical, tide-dominated semi-enclosed bay in China's Beibu Gulf, represents one such understudied system where mangrove evolution may follow different patterns due to its unique geomorphic and hydrodynamic setting.

Mangroves, characterized by their dense woody canopies (Duke and Schmitt, 2015), present significant challenges for traditional field-based monitoring, which is often labor-intensive and limited in spatial and temporal coverage (Maurya et al., 2021). The advent of remote sensing technology has revolutionized mangrove mapping, enabling long-term, large-scale assessments with improved accuracy (Vaiphasa et al., 2007). Recent advancements in image processing and machine learning classification algorithms have further enhanced the efficiency and precision of mangrove extraction (Giri, 2016).

Among various classification methods, the Random Forest (RF) algorithm has emerged as a particularly effective tool for mangrove mapping due to its robust performance in feature extraction and classification accuracy (Gilani et al., 2021). Applications of the RF algorithm have revealed significant spatiotemporal changes in mangrove ecosystems. For instance, in East Luwu, Indonesia, mangrove coverage dramatically declined from 4895.26 ha to 1730.24 ha between 2000 and 2015 (Jamaluddin et al., 2022). Conversely, along the Odisha coast of India, mangroves expanded from 222.43 ha to 252.47 ha from 2009 to 2019 (Parida and Kumar, 2020).

Given the success of machine learning approaches in mangrove monitoring, this study employs an RF-based classification framework to analyze the dynamic changes of mangroves in Fangcheng Bay (FCB), a subtropical, tide-dominated semi-enclosed bay in China's Beibu Gulf. This approach will provide critical insights into the spatiotemporal evolution of mangroves in this understudied coastal system.

FCB is located in the northern part of the Beibu Gulf, where mangrove resources are abundant (Tao et al., 2017). In recent years, with the rapid development of cities, the local mangroves may have suffered severe damage. However, little information is available regarding mangrove dynamics and possible driving factors in the FCB. The study utilized Landsat images, sea level data, hydrodynamic data, and inverted Suspended Sediment Concentration (SSC) to analyze the mangrove dynamics in the FCB. Furthermore, we explored the potential driving factors such as waves, sediment transport, and land-use changes. The main aims of this study were to 1) detect the dynamic changes of the mangrove area in the FCB from 1987 to 2023; 2) quantify the seaward expansion and landward side retreat of mangroves; 3) identify the main drivers affecting mangrove dynamics. This study contributes to a deeper understanding of the evolution of mangroves and their coupling relationships with both natural and human activities, providing essential theoretical references for the conservation and restoration of mangroves worldwide.

2. Materials and methods

2.1. Study area

FCB is located in the northern part of the Beibu Gulf, China, with its mouth facing south (Fig. 1A). Yuwan Island divides the FCB into the West Bay (WB) and the East Bay (EB). The tidal regime is classified as a mixed tide, with a maximum tidal range exceeding 4.5 m and a mean tidal range exceeding 2.1 m. The flood tide duration exceeds that of the ebb tide, with mean ebb velocities and flood velocities ranging from 20 to 50 cm/s and 30–75 cm/s, respectively (Luo and Ying, 1992). The wave directions were mainly from N (North) to NNE (North-Northeast) and ESE (East-Southeast) to S (South), with a mean height of 0.45 m (Fig. 1C and D). Meanwhile, FCB is a semi-enclosed bay where wave energy remains low due to the sheltering effect of flanking peninsulas (Luo and Ying, 1992). Consequently, tidal currents serve as the primary controlling factor for changes in sediment deposition within the bay. Located in the subtropical monsoon climate, the bay experiences simultaneous rainy and hot seasons. FCB contains abundant mangrove resources but exhibits a homogeneous species composition, with *Avicennia marina* as the dominant species (Tao et al., 2017). Here, the FCB was divided into the WB and the EB for the study (Fig. 1B).

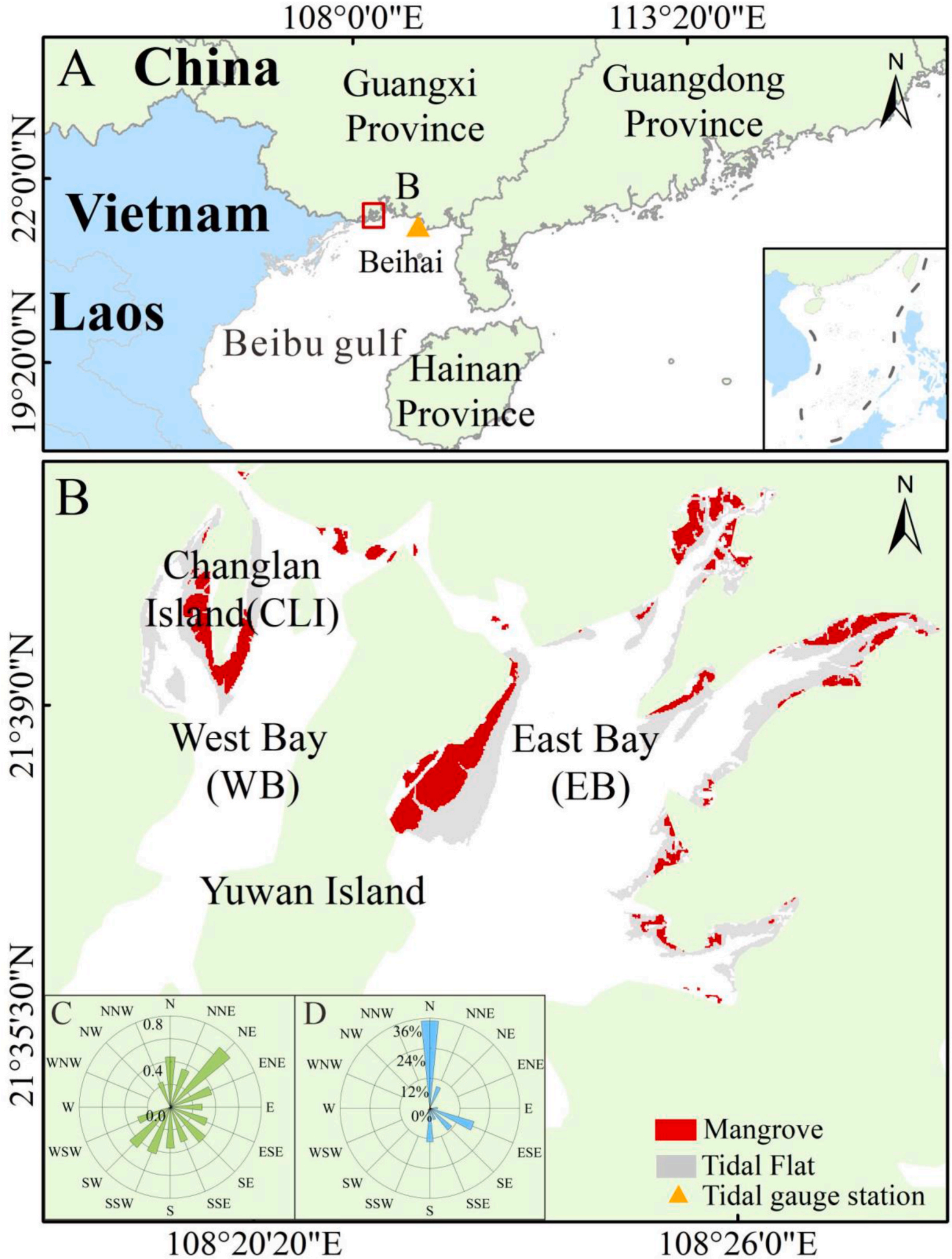

Fig. 1. Study area. (A) Location of the FCB. (B) Regional division in the FCB. (C) Average wave height in all directions. (D) Wave direction and frequency.

2.2. Materials

Landsat time-series remote sensing images were acquired from Google Earth Engine (https://earthengine.google.com) to extract mangroves and perform SSC inversion. Wave direction and mean wave height for FCB were acquired from *The Twelfth Volume of Chinese Gulf Record (Guangxi Gulf)* (Compilation Committee of China Gulf Record, 1993). Sea level data for Beihai were sourced from the South China Sea Branch of the State Oceanic Administration and the 2021 China Sea Level Bulletin (http://gi.mnr.gov.cn/202205/t20220507_2735509.html). Furthermore, we acquired a 3 arc-second global DEM (GDEM) with higher spatial resolution to calculate the average vertical sediment accumulation rate (Zhang et al., 2022).

2.3. Methods

2.3.1. Land class extraction

Machine learning has been widely applied to remote sensing image classification, with popular algorithms including Support Vector Machines, deep learning algorithms, and Random Forests (RF) (Mondal et al., 2019; Pashaei et al., 2020; Sheykhmousa et al., 2020). Support Vector Machines can work well with a small training dataset, but require substantial computational resources (Pal, 2009). Deep learning algorithms present remarkable capabilities in representation learning and model generalization (Talaei Khoei et al., 2023). However, their effectiveness is contingent upon the availability of large-scale datasets, and their practical application is constrained by inherent limitations in model interpretability (Talaei Khoei et al., 2023). Compared to other algorithms, RF demonstrates flexibility in handling various types of data analysis due to its high computational efficiency and classification accuracy (Jia et al., 2019; Yang and Huang, 2021; Rodriguez-Galiano et al., 2012). Additionally, RF can provide feature importance evaluation, aiding in the understanding of classification results (Belgiu and Drăgut, 2016). Consequently, RF exhibits high efficacy in mangrove identification (Aviña-Hernández et al., 2023). This study employs the RF to extract mangroves and other land cover types from remote sensing images, with a focus on mangrove dynamics in the FCB.

The Google Earth Engine (GEE) platform provides various multi-source remote sensing datasets (Gorelick et al., 2017). We used it to retrieve the Landsat surface reflectance dataset for FCB from 1987 to 2023, which had undergone both radiometric and atmospheric corrections, with all images having less than 30 % cloud cover, and exposed tidal flats (Amani et al., 2020). The reflectance of red, green, blue, near-infrared, and shortwave infrared bands was selected, along with the normalized difference vegetation index (NDVI), enhanced vegetation index (EVI), land surface water index (LSWI), modified normalized difference water index (MNDWI), and mangrove forest index (MFI), as classification input parameters (Wang et al., 2025) (Table 1). Classification samples include construction land and bare land, water, aquaculture ponds, mangroves, tidal flats, cultivated land, and woodland. These classification samples, spectral bands, and calculated indices were input into an RF classifier, producing classification results (Breiman, 2001). Furthermore, the overall accuracy and Kappa coefficient were employed as evaluation metrics to evaluate classification reliability (Chen et al., 2025). From 1987 to 2023, the overall accuracy and Kappa coefficient in all classified land cover types exceeded 88 % and 0.88, respectively, suggesting a reliable classification of the Landsat images used in this study.

2.3.2. Extraction of mangrove forests shoreline

The Digital Shoreline Analysis System, a powerful ArcGIS extension, is widely used to analyze mangrove shoreline dynamics (L'opez and Cellone, 2022). It provides a systematic approach to analyzing shoreline changes through a variety of statistical metrics, such as linear regression rate, endpoint rate (EPR) (Himmelstoss et al., 2021). The linear regression rate, determined by fitting a least-squares regression line to shoreline data points, provides a robust measure of coastal change (O'Brien et al., 2014; Wu et al., 2025b). This method requires a minimum of three shoreline positions for calculation. While effective for identifying linear trends, this approach has inherent limitations in capturing temporal variations in shoreline dynamics, as it assumes a constant rate of change throughout the observation period (Farris et al., 2023; O'Brien et al., 2014). Compared to the linear regression rate, EPR calculates the rate by dividing the net change between the two shorelines by the elapsed time period. This method is computationally straightforward and achieves high accuracy (O'Brien et al., 2014). Therefore, this study applies the EPR method to analyze mangrove shoreline changes in FCB from 1987 to 2023. Based on the training sample categories from FCB, mangrove shorelines for the years 1987, 1992, 1997, 2002, 2007, 2013, 2017, and 2023 were extracted using ArcGIS 10.8 software (Wang et al., 2025). Subsequently, the Digital Shoreline Analysis System software was used to analyze the expansion and erosion rates of the FCB mangrove shoreline (Himmelstoss et al., 2021). A total of 545 transects were generated, each spaced 100 m apart and numbered clockwise. The numbering ranges for the WB and EB in the FCB were 1–113 and 114–545, respectively. The rate of mangrove shoreline changes for each transect was expressed as EPR. Negative rates ($EPR<0$) indicate shoreline erosion (landward movement), while positive rates ($EPR>0$) indicate shoreline expansion (seaward movement) (Besset et al., 2019).

The Net Shoreline Movement (NSM) and EPR for each transect between 1987 and 2023 were calculated using Digital Shoreline Analysis System software (Wu et al., 2025a). Subsequently, the area of seaward mangrove expansion in the FCB was calculated based on the net shoreline movement and the distances between the transects. The calculation formula is as follows (Himmelstoss et al., 2021):

$$\mathrm{Area}_{gian} = \mathrm{NSM}_{\mathrm{EPR}>0} \mathrm{D}_{\mathrm{T}} \tag{1}$$

where D_T represents the transect spacing, set at 100 m, and NSM $_{EPR>0}$ is the NSM when the shorelines of 1987 and 2023 move seaward ($EPR > 0$).

To compare with sea level rise to determine the possible impacts of mangroves, the calculation of the average vertical sediment accumulation (AVSA) was used as an evaluation metric (Wang et al., 2025). The formula is as follows (Xiong et al., 2024):

$$\mathrm{AVSA} = \mathrm{V} \tan \theta \tag{2}$$

where V is the average accretion rate of shorelines, and θ is the average slope in the FCB obtained from Zhang et al. (2022).

2.3.3. Calculation of land use type transitions

Land use type transfer analysis reveals the conversion patterns among regional land types, reflecting changes in land use before and after the study period (Chen et al., 2023; Long and Qu, 2018). To assess mangrove gains and losses during different periods, the Intersect and Erase functions in ArcGIS 10.8 can be used for calculation (Li et al., 2026). The spatial overlay results of land types were further analyzed using the Intersect tool in ArcGIS 10.8 to determine the encroachment relationships among different land types (Sofue et al., 2025). Based on these operations, this study employed ArcGIS 10.8 to calculate the area of other land types encroaching on mangroves and the area of mangroves expanding into other land types.

2.3.4. Satellite data and processing

Remote sensing images with high spatial resolution and wide coverage are effective for monitoring water bodies (Ma et al., 2022; Katlane et al., 2013). In particular, Landsat remote sensing images are widely used for long-term monitoring of water bodies due to their continuous temporal coverage and spatiotemporal consistency (Wang

Table 1
Spectral indices for classification.

Name	Equation	References
Normalized Difference Vegetation Index(NDVI)	$\mathrm{NDVI} = \frac{(\rho_{nir} - \rho_{red})}{(\rho_{nir} + \rho_{red})}$	Rouse et al. (1974)
Enhanced Vegetation Index (EVI)	$\mathrm{EVI} = 2.5 \times \frac{(\rho_{nir} - \rho_{red})}{(\rho_{nir} + 6\rho_{red} - 7.5\rho_{blue} + 1)}$	Huete et al. (2002)
Land Surface Water Index (LSWI)	$\mathrm{LSWI} = \frac{(\rho_{nir} - \rho_{swir})}{(\rho_{nir} + \rho_{swir})}$	Chandrasekar et al. (2010)
Modified Normalized Difference Water Index (MNDWI)	$\mathrm{MNDWI} = \frac{(\rho_{green} - \rho_{swir})}{(\rho_{green} + \rho_{swir})}$	Xu (2006)
Mangrove Vegetation Index (MVI)	$\mathrm{MVI} = \frac{\rho_{nir} - \rho_{green}}{\rho_{swir1} - \rho_{green}}$	Baloloy et al. (2020)

et al., 2022; Zhou et al., 2023). We used a total of 841 images from the TM, ETM+, and OLI sensors from 1987 to 2023 to estimate the SSC in the FCB. All images underwent atmospheric and radiometric correction, with cloud detection and masking performed using the CFMask algorithm (Dwyer et al., 2018). Meanwhile, the focal statistics method was applied to fill the gaps in Landsat 7 ETM + images (Qian et al., 2012; Potić, 2015).

2.3.5. SSC retrieval models and model evaluation metrics

The Nechad model is a multi-sensor model based on single-band data, with strong adaptability to various water bodies and sensor types (Nechad et al., 2010; Dogliotti et al., 2015). It has been widely used for SSC estimation in estuarine waters, such as the Yangtze River and Pearl River estuaries, due to its high accuracy and flexibility in SSC inversion (Zhou et al., 2023; Garcia-Tunon et al., 2024). The model formulation is as follows (Nechad et al., 2010):

$$SSC = \frac{A_\rho(\lambda)\rho(\lambda)}{\left[1 - \frac{\rho(\lambda)}{C_\rho}(\lambda)\right]} + B_\rho(\lambda) \tag{3}$$

$$\rho(\lambda) = \pi R_{rs}(\lambda) \tag{4}$$

$A_\rho(\lambda)$, $B_\rho(\lambda)$, $C_\rho\lambda)$ are dimensionless variablesat the wavelength λ, and R_{rs} is the remote sensing reflectance at the wavelength λ. According to Novoa et al. (2017), the parameters as $A_\rho\lambda) = 477$, $B_\rho\lambda) = 0$, $C_\rho\lambda) = 0.1686$.

To evaluate the degree of correlation between in situ SSC and model-retrieved SSC, the determination coefficient (R^2) and the root mean square error (RMSE) were employed (Yang et al., 2025; Peterson et al., 2018). RMSE and R^2were 7.18 mg/L and 0.89, respectively. The RMSE formulation is as follows (Malik et al., 2017):

$$RMSE = \sqrt{\frac{1}{n}\sum_{i=1}^{n}(y_i - y_i')^2} \tag{5}$$

y_i' represents the in situ SSC, y_i denotes the estimated SSC, and n is the sample size. The higher the RMSE, the lower the SSC model accuracy.

2.3.6. In situ data collection

In situ suspended sediment concentration (SSC) measurements were collected from FCB coinciding with the Landsat 8 overpass on September 29, 2024. At each of the 10 sampling sites, 0.5 L water samples were obtained from a depth of 0.5 m below the water surface (Jiang et al., 2024). Following standardized protocols, the samples were filtered, oven-dried, and gravimetrically analyzed to determine SSC values (Du et al., 2022; Bayram et al., 2012). These field-measured data were subsequently used to validate the satellite-derived SSC retrieval model.

3. Results

3.1. Changes in mangrove forest areas

From 1987 to 2023, the mangrove forest area in FCB expanded significantly from 233.19 ha to 658.49 ha, exhibiting three distinct

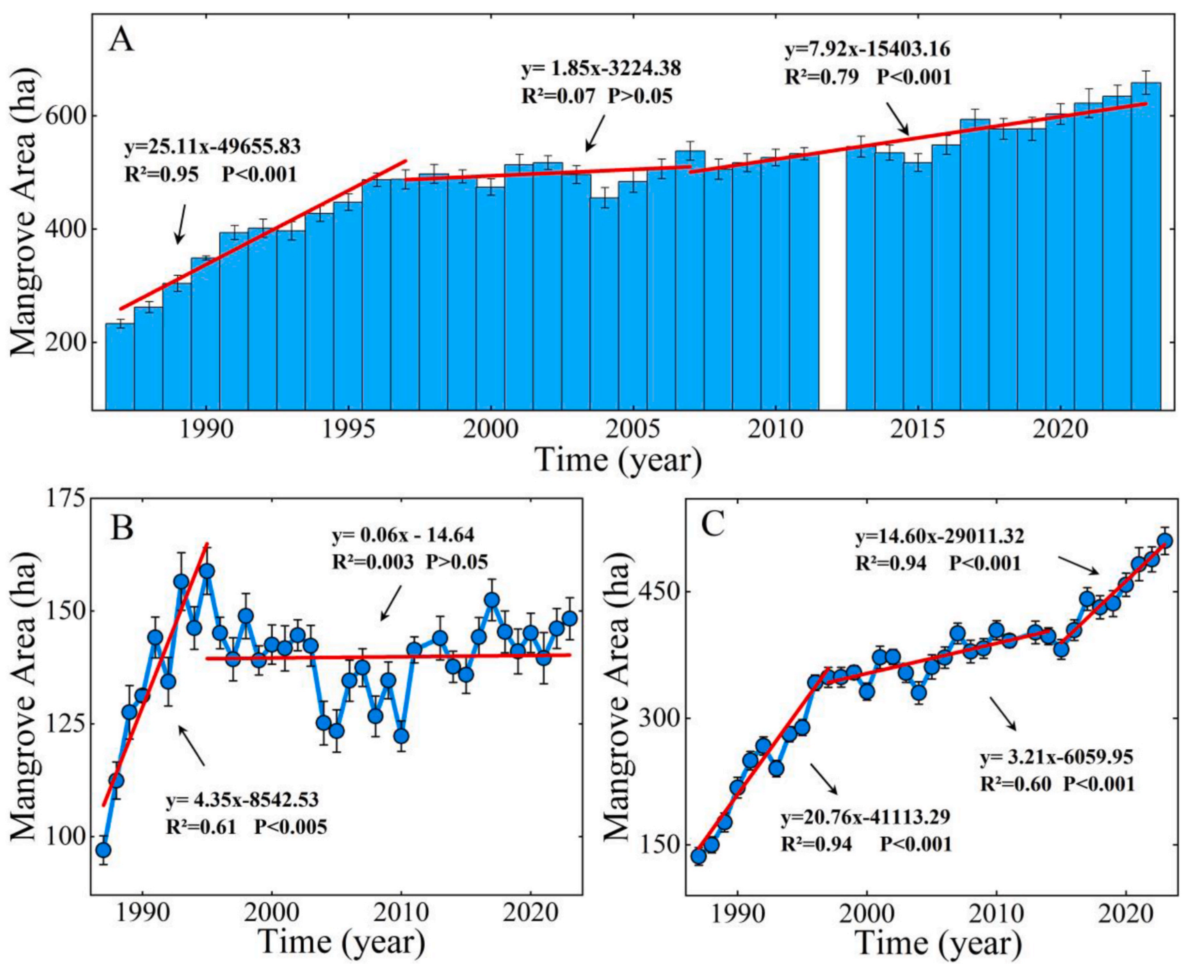

Fig. 2. Temporal changes in mangrove areas of the FCB and its various regions from 1987 to 2023 (The regression equation shows the linear relationship between time and mangrove area, where higher R^2values indicate a better fit and $p < 0.05$ indicates statistical significance). (A) In the FCB. (B) In the WB. (C) In the EB.

phases of change (Fig. 2). Specifically, from 1987 to 1997, the mangrove area expanded from 233.19 ha to 487.85 ha, with a significant growth rate of 25.11 ha/yr. Between 1997 and 2007, the mangrove area stagnated. From 2007 to 2023, the mangrove area resumed growth, increasing from 538.1 ha to 658.49 ha, with a growth rate of 7.92 ha/yr (Fig. 2A). However, the mangrove area in different regions within the FCB showed distinct variations. In 1987, the mangrove areas in the EB and WB accounted for 58.42 % and 41.58 % of the total mangrove area, respectively. By 2023, these proportions had changed to 77.47 % and 22.53 %, respectively (Fig. 2B and C). In the WB, from 1987 to 1995, the mangrove area increased from 96.95 ha to 158.89 ha, with a growth rate of 4.35 ha/yr. Between 1995 and 2023, the mangrove forest area exhibited remarkable stability, showing minimal fluctuations (Fig. 2B). Compared to the WB, the mangroves in the EB showed a continuous growth trend. The mangrove area increased from 136.24 ha in 1987 to 348.53 ha in 1997, with a growth rate of 20.76 ha/yr. From 1997 to 2015, the mangrove area expanded from 348.53 ha to 381.62 ha, with a growth rate of 3.21 ha/yr. Between 2015 and 2023, the mangrove area further increased from 381.62 ha to 510.18 ha, with a growth rate of 14.60 ha/yr (Fig. 2C).

3.2. Spatial dynamics in mangrove forest

From 1987 to 2023, mangrove expansion in FCB exhibited distinct spatial patterns, with most growth occurring within the bay while remaining virtually absent near the mouth (Fig. 3). However, WB and EB displayed divergent change patterns. Initial conditions in 1987 revealed a concentrated mangrove area of 75.77 ha in the CLI, contrasting with only 19.41 ha of dispersed mangroves across the eastern and northern tidal flats (Fig. 3A). Subsequently, the mangroves in the eastern tidal flats gradually disappeared, with 11.08 ha of mangroves lost by 1997 (Fig. 3C). Conversely, the mangroves in the CLI and northern tidal flats expanded both landward and seaward from 1987 to 1997 (Fig. 3A–C). The expansion of mangroves in the CLI was particularly evident, with the mangrove area increasing to 111.33 ha, accounting for 79.91 % of the total mangrove area (Fig. 3A–C). However, from 1997 to 2002, the scattered mangrove patches on the landward side of CLI disappeared (Fig. 3C and D). From 2002 to 2023, mangroves in the northern tidal flats expanded slowly from the original patches, while landward mangroves in CLI continued to decline, with the seaward side maintaining a slow expansion trend (Fig. 3D–H).

From 1987 to 1997, mangrove patches appeared in the eastern tidal flats, and the mangroves in the northern tidal flats began to encroach upon tidal channels (Fig. 3A–C). Meanwhile, the mangroves in the western tidal flats rapidly expanded toward the northern and southern tidal flats, merging into a contiguous mangrove patch that accounted for 56.30 % of the total mangrove area in 1997 (Fig. 3A–C). However, the mangroves began to disappear on the landward side of the southwest part after 1992, with a loss of 78.74 ha by 2013 (Fig. 3B–F). From 2013 to 2023, the mangroves generally exhibited seaward expansion as a whole. Furthermore, the mangroves in the northern tidal flats continued to grow along the tidal channels, with an increase of 70.31 ha in area

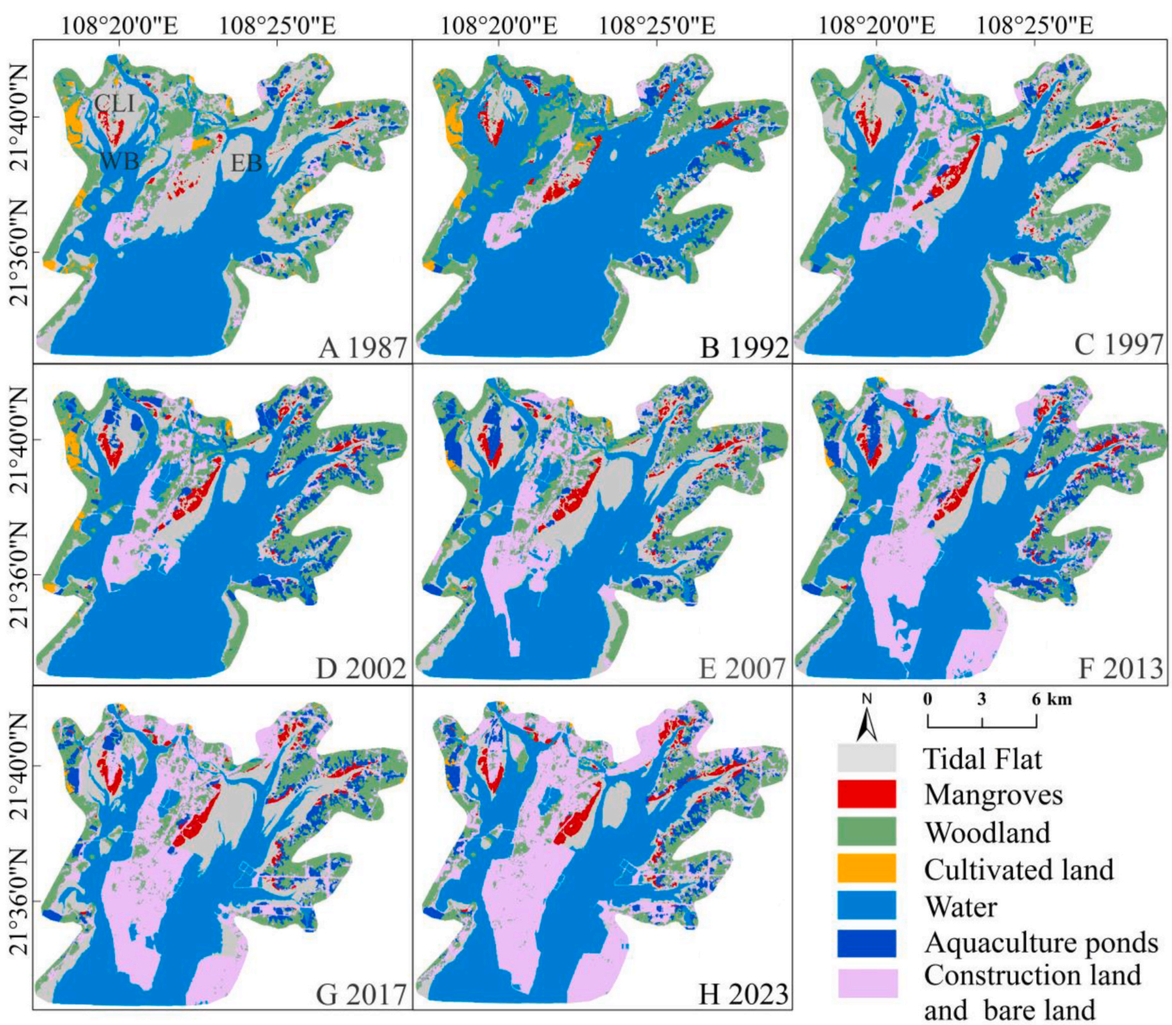

Fig. 3. The spatial dynamics of mangroves in the FCB from 1987 to 2023.

(Fig. 3F–H).

3.3. Shoreline changes of the mangrove forest

From 1987 to 2023, the mangrove shorelines in the FCB expanded seaward by 267.99 ha, with an average overall migration rate of 1.28 m/yr (Fig. 4A). The expansion and erosion transects accounted for 84.04 % and 15.96 % of all transects, with average change rates of 2.17 m/yr and −3.48 m/yr, respectively (Fig. 4B). Specifically, the mangroves in the WB expanded seaward by 41.14 ha, with an average change rate of 0.87 m/yr. The transects of expansion and erosion accounted for 69.03 % and 30.97 %, respectively (Fig. 4B). Compared to the WB, from 1987 to 2023, the mangrove in the EB expanded seaward by 226.85 ha, with an average change rate of 1.39 m/yr. The expansion transects accounted for 87.96 %, with an average change rate of 2.22 m/yr. The erosion transects accounted for 12.04 %, with an average change rate of −4.65 m/yr. Mangrove erosion primarily occurred in the southwest of the EB, with a maximum erosion rate of −11.57 m/yr (Fig. 4B).

3.4. Conversion between mangroves and other land cover types

From 1987 to 2023, a total of 354.20 ha of mangroves were lost in FCB, mainly occurring on the landward side. The areas of mangroves converted into woodland, cultivated land, construction land and bare land, aquaculture ponds, and tidal flats were 32.86, 0.66, 125.56, 78.87, and 116.25 ha, respectively, accounting for 9.28 %, 0.18 %, 35.45 %, 22.27 % and 32.82 % of the total mangrove loss area (Fig. 5). Specifically, from 1987 to 1992, the encroachment of other land cover types on mangroves was relatively minor, with only 15.24 ha of mangrove lost. The loss of mangroves was most notable between 1992 and 2013, accounting for 75.03 % of the loss during this period, totaling 265.77 ha. The highest proportion of mangrove conversions was into construction land and bare land, aquaculture ponds, and tidal flats, accounting for 35.58 %, 24.26 %, and 34.24 % of mangrove loss during this period, respectively. From 2013 to 2023, mangrove loss has significantly decreased. The mangrove continues to be primarily converted into construction land and bare land, aquaculture ponds, and tidal flats, accounting for 51.78 %, 13.42 %, and 22.41 % of the total mangrove loss area, respectively.

The areas of woodland, cultivated land, construction land and bare land, aquaculture ponds, and tidal flats in FCB converted into mangroves between 1987 and 2023 were 27.39, 1.08, 23.34, 58.37, and 669.32 ha, respectively, accounting for 3.51 %, 0.14 %, 2.99 %, 7.49 % and 85.87 % of the total mangrove expansion area (Fig. 6). Specifically, from 1987 to 1992, mangrove expanded rapidly, largely attributed to the transformation of extensive tidal flat areas into mangroves, which accounted for 98.59 % of the increase in mangrove area during this period. However, between 1992 and 2007, the expansion area of mangroves was gradually decreasing. The expansion is still primarily driven by the conversion of tidal flats to mangroves, which accounted for 93.37 % of the increase in mangrove area during this period. From 2007 to 2023, the area of mangrove expansion gradually increased, with the conversions from tidal flats, aquaculture ponds, construction land and bare land, and woodland contributing 66.88 %, 18.6 %, 7.85 %, and 6.67 %, respectively, to the total mangrove expansion during this period.

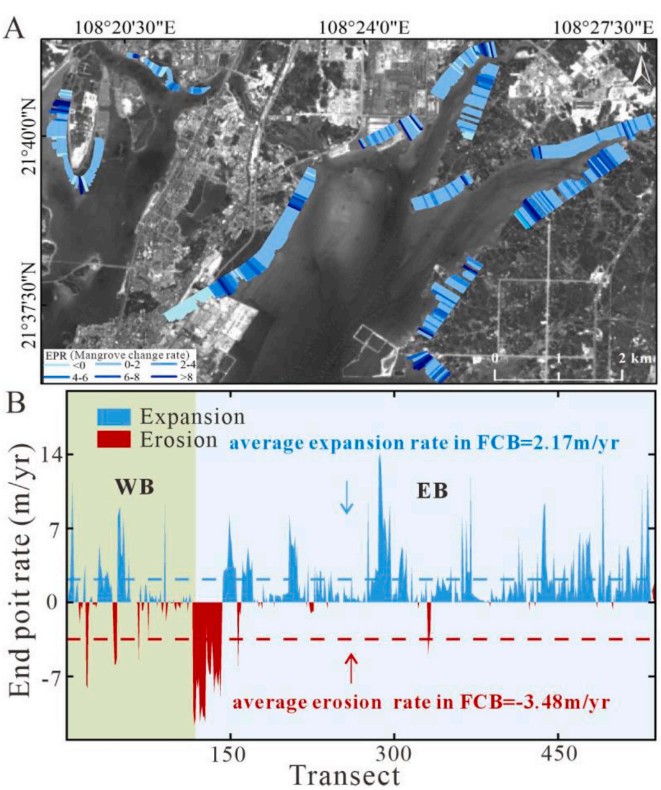

Fig. 4. (A) The expansion and erosion of the mangrove shoreline of the FCB from 1987 to 2023. (B) Quantitative analysis of shoreline expansion and erosion of the FCB from 1987 to 2023.

4. Discussion

4.1. Impacts of local suspended sediment concentration

The sufficient suspended sediment facilitates tidal flat progradation, enabling mangrove habitat expansion (Adame et al., 2010; Besely et al., 2021). Conversely, sediment deficiency may inhibit mangrove expansion or trigger habitat loss (Worthington et al., 2020). Over the past few decades, river discharge and SSC of major rivers flowing into the Beibu Gulf have significantly decreased due to the construction of dams and reservoirs, reducing the transport of suspended sediments to the ocean (Li et al., 2022; Gao et al., 2015; Gao et al., 2024). However, the mangroves in FCB continued to expand seaward, and the decline in SSC did not cause loss of mangroves (Figs. 4 and 7). A similar phenomenon was also observed in the Red River Delta, where mangroves continue to expand toward the sea despite the decrease in suspended sediment discharge (Long et al., 2021). It indicates that the current decrease in SSC within the bay has not yet impeded the seaward progression of mangroves.

4.2. Estuarine hydrodynamics

Tidal currents continuously transport sediments to mangrove tidal flats, providing the material foundation for mangrove establishment and expansion (Woodroffe et al., 2016; Bryan et al., 2017). Here, the main tidal currents flow in the EB, while the rest of the tides flow to the WB (Luo and Ying, 1992). The stronger tidal sediment transport capacity of EB accelerated sediment accumulation, resulting in a wider and gentler intertidal surface compared with the WB (Gao and Zhou, 2023; Luo and Ying, 1992). Furtherly, the mangroves in this region are more easily colonized and further promote sediment deposition, driving their migration toward bare tidal flats (Fig. 4). This pattern of mangrove expansion is similar to that observed in the Nanliu River Delta (Long et al., 2022). Furthermore, sustained tidal sediment transport has facilitated tidal channel development and driven the expansion of mangroves in the northeast of the EB along the tidal channel (Zhou et al., 2024) (Fig. 3), which is similar to the expansion pattern of mangroves in the Beilun Estuary and the Indian Delta (Zhou et al., 2024; Long et al., 2025). Therefore, the stronger tidal sediment transport in the EB results in a faster expansion of mangrove forests than in the WB.

Meanwhile, mangroves typically grow in shallow coastal waters and are susceptible to wave action (Nguyen et al., 2013). However, the low wave energy environment in FCB provides favorable conditions for the

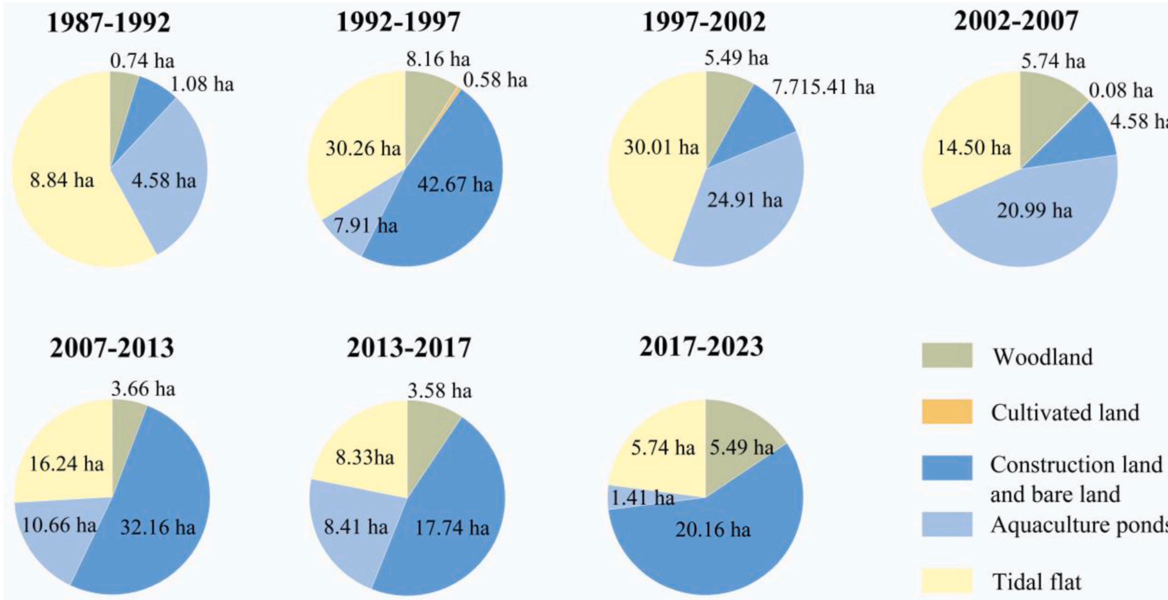

Fig. 5. The area of mangroves converted to other land types in the FCB from 1987 to 2023.

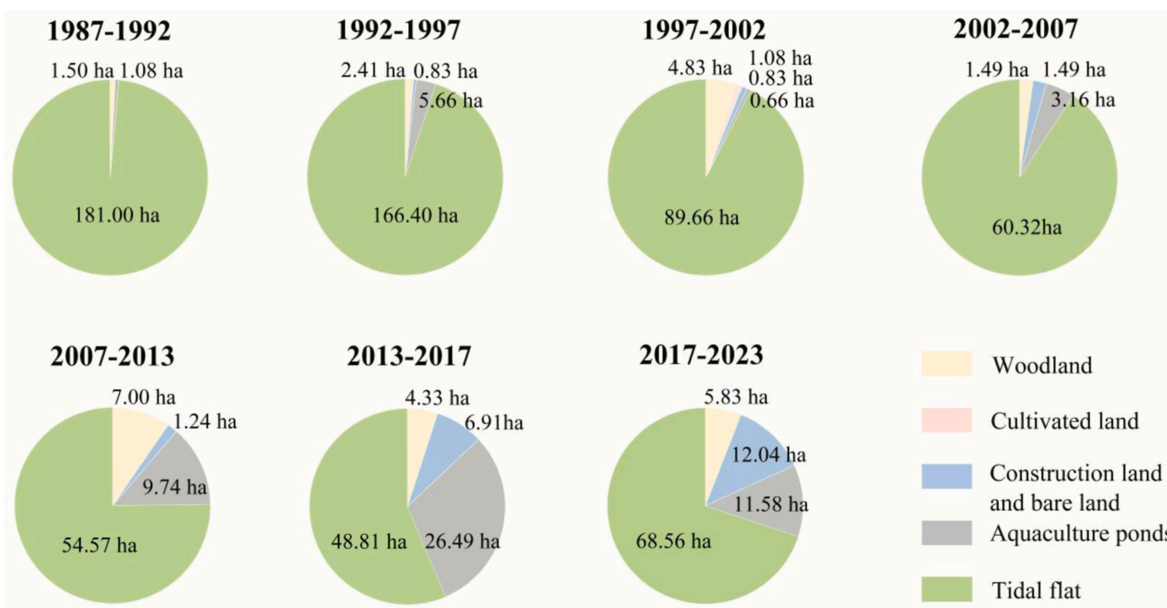

Fig. 6. The area of other land types converted to mangroves in the FCB from 1987 to 2023.

expansion of mangroves. The wave directions in FCB were mainly from the N (North) to NNE (North-Northeast) and ESE (East-Southeast) to S (South) (Luo and Ying, 1992), while the mangroves primarily grow along the northern shoreline, adjacent to the terrestrial boundaries (Fig. 3). Since the seaward side of the mangroves is not directly aligned with the wave propagation paths from the N (North) to NNE (North--Northeast), the mangroves are effectively shielded from the impact of waves (Luo and Ying, 1992). Moreover, the flanking peninsulas provide significant sheltering effects against waves from the ESE (East--Southeast) to S (South), further reducing the interference of waves on mangroves (Huang et al., 2022) (Fig. 1D). In contrast, mangroves in the Fly River Delta and the Irrawaddy River Delta are directly exposed to high wave energy, leading to mangroves uprooting (Wu et al., 2025b; Xiong et al., 2024). Furthermore, the sea level rose significantly at a rate of 0.188 cm/yr from 1987 to 2021, while the average vertical sediment accumulation rate was 2.3 cm/yr, and the mangroves also exhibited a pronounced seaward expansion trend. This means that sea level rise has not yet affected the seaward expansion of mangroves in the FCB.

4.3. Anthropogenic activities

Anthropogenic disturbances of high intensity, such as land reclamation, mudflat economy, and aquaculture ponds, have caused severe loss of mangrove forests in the Beibu Gulf (Jia et al., 2014; Gao et al., 2025), which is consistent with the results of this study (Fig. 5). Since the 1990s, large-scale land reclamation and saltpan development have been carried out in FCB to promote economic growth, leading to extensive mangrove deforestation and a significant increase in the area of mangrove loss (Lu et al., 2023; Jiang et al., 2022; Jia et al., 2014). Additionally, the aquaculture industry developed rapidly during this period (Duan et al., 2021). Given its higher economic value, many farmers clear mangroves for expanding aquaculture operations, further

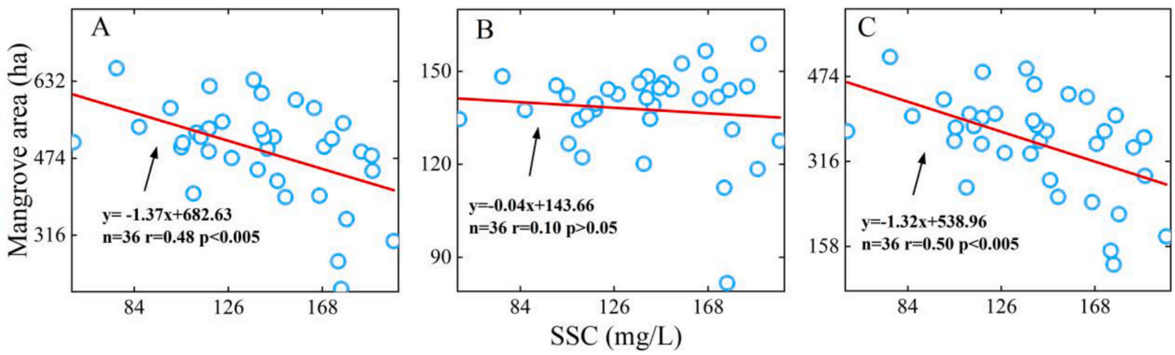

Fig. 7. The SSC in the FCB and the relationships between the mangrove area and SSC in different regions from 1987 to 2023 (The linear fitting equation describes the correlation between SSC and mangrove area, where r indicates the correlation coefficient, n is the sample size, and $p < 0.05$ indicates statistical significance). (A) In the FCB. (B) In the WB. (C) In the EB.

accelerating the degradation of landward mangroves (Jiang et al., 2022; Gao et al., 2025).

As awareness regarding the significance of mangrove ecosystems deepens, a series of relevant laws has been formulated to protect mangroves by the government since 2010 (Sun et al., 2024; Jia et al., 2014). The implementation of these policies effectively curbed the degradation of mangroves and gradually improved the ecological environment conditions, creating a favorable foundation for the expansion of mangroves (Arifanti et al., 2022; Alongi, 2008; Jia et al., 2014). On this basis, FCB has further promoted the restoration and expansion of mangroves towards the sea by establishing a mangrove protection park and large-scale afforestation (Figs. 4 and 6), indicating that the sustained mangrove protection efforts can mitigate or even offset the negative impacts caused by human activities on mangroves. This phenomenon of mangrove expansion under strong anthropogenic pressure has also been observed in the Dandou Sea, Beilun Estuary, and Nanliu River Delta of the Beibu Gulf, indicating the effectiveness and regional applicability of mangrove conservation measures (Wu et al., 2025a; Long et al., 2022, 2025).

With the continued implementation of mangrove conservation measures, the mangroves in the Beibu Gulf of China are expected to keep expanding in the coming decades (Zhang et al., 2025), accompanied by simultaneous increases in regional carbon storage capacity and biodiversity levels (Doughty et al., 2016; Nagelkerken et al., 2008). Currently, China is implementing systematic strategies to enhance blue carbon ecosystems and biodiversity conservation (Yu and Wang, 2023). The FCB mangrove case study demonstrates remarkable resilience, maintaining expansion trajectories despite persistent anthropogenic pressures. This paradigm offers valuable guidance for optimizing coastal zone management to achieve dual biodiversity-carbon objectives across China's maritime territories in the climate change era.

4.4. Uncertainty analysis

This study lacks available remote sensing images for 2012 because the Landsat-7 ETM + experienced a failure of its Scan Line Corrector mechanism, affecting the continuity of long-term trend assessments (Hossain et al., 2015; Chen et al., 2012). Furthermore, the wave data from the Twelfth Volume of Chinese Gulf Record (Guangxi Gulf) (Compilation Committee of China Gulf Record, 1993) provide reliable insights. However, they may exhibit systematic biases during anomalous climate events, which could influence the conclusions regarding the effects of hydrodynamics on mangroves.

5. Conclusions

Mangroves are among the most valuable ecosystems in terms of ecological services, providing significant ecological, economic, and social benefits. In this study, we employed the random forest algorithm and remote sensing imagery to analyze mangrove dynamics in the FCB from 1987 to 2023 and to explore the reasons and outcomes behind these changes. The main findings are as follows:

1. The mangrove area in FCB exhibited three distinct growth phases: (1) rapid expansion (1987–1997), characterized by a 109.21 % increase in coverage; (2) stagnation (1997–2007), with minimal areal changes; and (3) gradual recovery (2007–2023), showing a 30.17 % increase.
2. Seaward mangrove expansion accounted for 267.99 ha of net area gain, while landward margins experienced concentrated losses, demonstrating distinct spatial patterns of mangrove dynamics.
3. The decline in SSC did not inhibit mangrove seaward expansion, as tidal currents sustained sediment supply to intertidal zones, creating suitable substrates for mangrove colonization.
4. Land reclamation, mudflat development, and aquaculture pond construction are the main factors contributing to mangrove loss in FCB.

CRediT authorship contribution statement

Xiaowen Xie: Writing – review & editing, Writing – original draft, Software, Resources, Methodology, Investigation. **Zhijun Dai:** Writing – review & editing, Writing – original draft, Resources, Project administration, Methodology, Investigation, Funding acquisition, Formal analysis, Data curation, Conceptualization. **Riming Wang:** Writing – review & editing, Writing – original draft, Methodology, Investigation, Funding acquisition. **Tianliang Wu:** Resources, Project administration, Methodology, Investigation, Formal analysis. **Baoqing Hu:** Visualization, Validation, Software, Resources, Formal analysis. **Xixing Liang:** Investigation, Formal analysis, Data curation.

availability statement

Landsat time-series remote sensing images were acquired from Google Earth Engine (https://earthengine.google.com). Sea level data for Beihai were sourced from the South China Sea Branch of the State Oceanic Administration and the 2021 China Sea Level Bulletin (http://gi.mnr.gov.cn/202205/t20220507_2735509.html). Wave direction and mean wave height for FCB were acquired from The Twelfth Volume of Chinese Gulf Record (Guangxi Gulf) (Compilation Committee of China Gulf Record, 1993).

Declaration of competing interest

The authors declare that there are no conflicts of interest regarding the submitted paper of "Machine learning-based detection of mangrove dynamics in a subtropical bay: reasons and outcomes".

Acknowledgments

This research was supported by the National Natural Science Key Foundation of China (NSFC) (41930537), National Natural Science Key Foundation of China (NSFC) (42366009), Shanghai International Science and Technology Cooperation Fund Project (23230713800, 24230740100), and the Marine Science Program for Guangxi First-Class Discipline, Beibu Gulf University. We are grateful to anonymous reviewers for their constructive comments and suggestions that improved the article.

Data availability

Data will be made available on request.

References

Alongi, D.M., 2002. Present state and future of the world's mangrove forests. Environ. Conserv. 29 (3), 331–349.
Adame, M.F., Neil, D., Wright, S.F., Lovelock, C.E., 2010. Sedimentation within and among mangrove forests along a gradient of geomorphological settings. Estuar. Coast Shelf Sci. 86 (1), 21–30.
Amani, M., Ghorbanian, A., Ahmadi, S.A., Kakooei, M., Moghimi, A., Mirmazloumi, S.M., 2020. Google Earth engine cloud computing platform for remote sensing big data applications: a comprehensive review. IEEE J-stars 13, 5326–5350.
Alongi, D.M., 2008. Mangrove forests: resilience, protection from tsunamis, and responses to global climate change. Estuar. Coast Shelf Sci. 76 (1), 1–13.
Arifanti, V.B., Kauffman, J.B., Subarno, Ilman, M., Tosiani, A., Novita, N., 2022. Contributions of mangrove conservation and restoration to climate change mitigation in Indonesia. Glob. Change Biol. 28 (15), 4523–4538.
Aviña-Hernández, J., Ramírez-Vargas, M., Roque-Sosa, F., Martínez-Rincón, R.O., 2023. Predictive performance of random forest on the identification of mangrove species in arid environments. Ecol. Inform. 75, 102040.
Berger, U., Rivera-Monroy, V.H., Doyle, T.W., Dahdouh-Guebas, F., Duke, N.C., Fontalvo-Herazo, M.L., Hildenbrandt, H., Koedam, N., Mehlig, U., Piou, C., Twilley, R.R., 2008. Advances and limitations of individual-based models to analyze and predict dynamics of mangrove forests: a review. Aquat. Bot. 89 (2), 260–274.
Bessely, S.M., van der Wegen, M., Grueters, U., Reyns, J., Dijkstra, J., Roelvink, D., 2021. Eleven years of mangrove-Mudflat dynamics on the mud volcano-induced prograding delta in East Java, Indonesia: integrating UAV and satellite imagery. Remote Sens. 13 (6), 1084.
Bunting, P., Rosenqvist, A., Hilarides, L., Lucas, R.M., Thomas, N., Tadono, T., Worthington, T.A., Spalding, M., Murray, N.J., Rebelo, L.M., 2022. Global mangrove extent change 1996-2020: global mangrove watch version 3.0. Remote Sens. 14 (15), 3657.
Baloloy, A.B., Blanco, A.C., Raymund Rhommel, R.R.C., Nadaoka, K., 2020. Development and application of a new mangrove vegetation index (MVI) for rapid and accurate mangrove mapping. ISPRS J. Photogrammetry Remote Sens. 166, 95–117.
Belgiu, M., Drăguţ, L., 2016. Random forest in remote sensing: a review of applications and future directions. ISPRS J. Photogrammetry Remote Sens. 114, 24–31.
Besset, M., Gratiot, N., Anthony, E.J., Bouchette, F., Goichot, M., Marchesiello, P., 2019. Mangroves and shoreline erosion in the Mekong River delta, Viet Nam. Estuar. Coast Shelf Sci. 226, 106263.
Breiman, L., 2001. Random forests. Mach. Learn. 45 (1), 5–32.
Bryan, K.R., Nardin, W., Mullarney, J.C., Fagherazzi, S., 2017. The role of cross-shore tidal dynamics in controlling intertidal sediment exchange in mangroves in Cù Lao Dung, Vietnam. Cont. Shelf Res. 147, 128–143.
Bayram, A., Kankal, M., Önsoy, H., 2012. Estimation of suspended sediment concentration from turbidity measurements using artificial neural networks. Environ. Monit. Assess. 184 (7), 4355–4365.
Crase, B., Liedloff, A., Vesk, P.A., Burgman, M.A., Wintle, B.A., 2013. Hydroperiod is the main driver of the spatial pattern of dominance in mangrove communities. Global Ecol. Biogeogr. 22 (7), 806–817.
Chen, L., Lin, Q., Krauss, K.W., Zhang, Y., Cormier, N., Yang, Q., 2021. Forest thinning in the seaward fringe speeds up surface elevation increment and carbon accumulation in managed mangrove forests. J. Appl. Ecol. 58 (9), 1899–1909.
Chandrasekar, K., Sai, M.V.R.S., Roy, P.S., Dwevedi, R., 2010. Land Surface Water Index (LSWI) response to rainfall and NDVI using the MODIS Vegetation Index product. Int. J. Rem. Sens. 31, 3987–4005.
Chen, C., Yang, X., Jiang, S., Liu, Z., 2023. Mapping and spatiotemporal dynamics of land-use and land-cover change based on the Google Earth Engine cloud platform from Landsat imagery: a case study of Zhoushan Island, China. Heliyon 9 (9), e19654.
Chen, L., Wang, W., Zhang, Y., Lin, G., 2009. Recent progresses in mangrove conservation, restoration and research in China. J. Plant Ecol. 2 (2), 45–54.
Compilation Committee of China Gulf Record, 1993. The Twelfth Volume of Chinese Gulf Record (Guangxi Gulf). Ocean Press, Beijing.
Cannon, D., Kibler, K., Donnelly, M., McClenachan, G., Walters, L., Roddenberry, A., Phagan, J., 2020. Hydrodynamic habitat thresholds for mangrove vegetation on the shorelines of a microtidal estuarine lagoon. Ecol. Eng. 158, 106070.
Chen, Y., Dai, Z., Mei, X., Huang, H., Cai, M., Xi, Y., Chen, R., 2025. Seaward expansion of mangrove wetlands in the Dafeng Estuary, Beibu Gulf from 1988 to 2022. Mar. Environ. Res., 107655
Chen, F., Zhao, X., Ye, H., Karakehayov, Z., 2012. Making use of the Landsat 7 SLC-off ETM+ image through different recovering approaches. Data Acquisition Applications 317–342.
Donato, D.C., Kauffman, J.B., Murdiyarso, D., Kurnianto, S., Stidham, M., Kanninen, M., 2011. Mangroves among the most carbon-rich forests in the tropics. Nat. Geosci. 4 (5), 293–297.
Dai, Z., Long, C., Mei, X., Fagherazzi, S., Xiong, Y., 2024. Overestimation of mangroves deterioration from sea level rise in tropical deltas. Geophys. Res. Lett. 51 (19) e2024GL109675.
Duke, N.C., Schmitt, K., 2015. Mangroves: unusual forests at the seas edge. Tropical forestry handbook 1.
Dwyer, J.L., Roy, D.P., Sauer, B., Jenkerson, C.B., Zhang, H.K., Lymburner, L., 2018. Analysis ready data: enabling analysis of the Landsat archive. Remote Sens. 10 (9), 1363.
Dogliotti, A.I., Ruddick, K.G., Nechad, B., Doxaran, D., Knaeps, E., 2015. A single algorithm to retrieve turbidity from remotely-sensed data in all coastal and estuarine waters. Rem. Sens. Environ. 156, 157–168.
Doughty, C.L., Langley, J.A., Walker, W.S., Feller, I.C., Schaub, R., Chapman, S.K., 2016. Mangrove range expansion rapidly increases coastal wetland carbon storage. Estuaries Coasts 39, 385–396.
Du, C., Li, Y., Lyu, H., Shi, K., Liu, N., Yan, C., Pan, J., Guo, Y., Li, Y., 2022. Characteristics of the total suspended matter concentration in the Hongze Lake during 1984-2019 based on landsat data. Remote Sens. 14 (12), 2919.
Duan, Y., Tian, B., Li, X., Liu, D., Sengupta, D., Wang, Y., Peng, Y., 2021. Tracking changes in aquaculture ponds on the China coast using 30 years of Landsat images. Int. J. Appl. Earth Obs. Geoinf. 102, 102383.
Friess, D.A., Rogers, K., Lovelock, C.E., Krauss, K.W., Hamilton, S.E., Lee, S.Y., Lucas, R., Primavera, J., Pajkaran, A., Shi, S., 2019. The state of the world's mangrove forests: past, present, and future. Annu. Rev. Environ. Resour. 44 (1), 89–115.
FAO, 2007. Food and Agriculture Organization of the United Nations in the world's mangroves 1980-2005. Forest Resources Division. FAO, Rome, Italy.
FAO, 2023. The World's Mangroves 2000-2020. FAO, Rome, Italy.
Farris, A.S., Long, J.W., Himmelstoss, E.A., 2023. Accuracy of shoreline forecasting using sparse data. Ocean Coast Manag. 239, 106621.
Gao, Y., Yu, G., Yang, T., Jia, Y., He, N., Zhuang, J., 2016. New insight into global blue carbon estimation under human activity in land-sea interaction area: a case study of China. Earth Sci. Rev. 159, 36–46.
Gilman, E., Ellison, J., Coleman, R., 2007. Assessment of mangrove response to projected relative sea-level rise and recent historical reconstruction of shoreline position. Environ. Monit. Assess. 124, 105–130.
Goldberg, L., Lagomasino, D., Thomas, N.M., Fatoyinbo, T.E., 2020. Global declines in human-driven mangrove loss. Glob. Change Biol. 26, 5844–5855.
Giri, C., Zhu, Z., Tieszen, L.L., Singh, A., Gillette, S., Kelmelis, J.A., 2008. Mangrove forest distributions and dynamics (1975-2005) of the tsunami-affected region of Asia. J. Biogeogr. 35 (3), 519–528.
Gilani, H., Naz, H.I., Arshad, M., Nazim, K., Akram, U., Abrar, A., Asif, M., 2021. Evaluating mangrove conservation and sustainability through spatiotemporal (1990-2020) mangrove cover change analysis in Pakistan. Estuarine, Coast. Shelf Sci. 249, 107128.
Gao, W., Lu, C., Yang, N., Wu, Y., Wu, K., Chen, Z., 2025. Cross-border mangrove dynamics and management in the Beibu Gulf: Long-term remote sensing observation using object-oriented deep learning. Ecol. Indic. 170, 113113.
Giri, C., 2016. Observation and monitoring of mangrove forests using remote sensing: opportunities and challenges. Remote Sens. 8 (9), 783.
Gorelick, N., Hancher, M., Dixon, M., Ilyushchenko, S., Thau, D., Moore, R., 2017. Google Earth Engine: Planetary-scale geospatial analysis for everyone. Rem. Sens. Environ. 202, 18–27.
Garcia-Tunon, W., Curra-Sánchez, E.D., Lara, C., González-Rodríguez, L., Urrego, E.P., Delegido, J., Broitman, B.R., 2024. Spatio-temporal variability of turbidity derived from Sentinel-2 in Reloncaví sound, Northern Patagonia, Chile. Ecol. Inform. 83, 102814.
Gao, J., Dai, Z., Mei, X., Ge, Z., Wei, W., Xie, H., Li, S., 2015. Interference of natural and anthropogenic forcings on variations in continental freshwater discharge from the Red River (Vietnam) to sea. Quat. Int. 380, 133–142.
Gao, E., Zhou, G., Li, S., Fu, B., Xiao, Y., Lan, Y., Wang, F., Xu, J., Zhu, Q., Bai, Y., 2024. Spatio-temporal evolution monitoring and analysis of tidal flats in Beibu Gulf from 1987 to 2021 using multisource remote sensing. IEEE J. Sel. Top. Appl. Earth Obs. Rem. Sens. 17, 6099–6114.
Gao, E., Zhou, G., 2023. Spatio-temporal changes of mangrove-covered tidal flats over 35 years using satellite remote sensing imageries: a case study of Beibu Gulf, China. Remote Sens. 15 (7), 1928.
Hogarth, P.J., 2015. The Biology of Mangroves and Seagrasses. Oxford university press.
Huete, A., Didan, K., Miura, T., Rodriguez, E.P., Gao, X., Ferreira, L.G., 2002. Overview of the radiometric and biophysical performance of the modis vegetation indices. Remote Sens. Environ. 83 (1–2), 195–213.
Himmelstoss, E.A., Henderson, R.E., Kratzmann, M.G., Farris, A.S., 2021. Digital Shoreline Analysis System (DSAS) Version 5.1 User Guide, pp. 51–52.
Hu, Z., Suzuki, T., Zitman, T., Uittewaal, W., Stive, M., 2014. Laboratory study on wave dissipation by vegetation in combined current-wave flow. Coast. Eng. 88, 131–142.

Hu, Z., Temmerman, S., Zhu, Q., Wang, X., Wu, J., Xu, T., Schoutens, K., Suzuki, T., Yang, Z., Bouma, T.J., 2025. Predicting nature-based coastal protection by mangroves under extreme waves. Proc. Natl. Acad. Sci. 122 (12), e2410883122.

Huang, Z., Zhou, X., Dai, Z., Che, Z., 2022. Analysis of the variations of suspended sediment concentration in vertical profile near the bed of Aegiceras corniculatum tidal flat. Journal of Tropical Oceanography 41 (4), 38–50, 2022.

Hossain, M.S., Bujang, J.S., Zakaria, M.H., Hashim, M., 2015. Assessment of the impact of Landsat 7 Scan Line Corrector data gaps on Sungai Pulai Estuary seagrass mapping. Applied Geomatics 7 (3), 189–202.

IUCN, 2024. The first-ever global assessment for the IUCN Red List of Ecosystems reveals that more than half of the world's mangroves are at risk of collapse by 2050. https://www.iucn.org/story/202405/first-ever-global-assessment-iucn-red-list-ecosystems-reveals-more-half-worlds.

Jia, M., Wang, Z., Mao, D., Ren, C., Song, K., Zhao, C., Wang, C., Xiao, X., Wang, Y., 2023. Mapping global distribution of mangrove forests at 10-m resolution. Sci. Bull. 68 (12), 1306–1316.

Jia, M., Wang, Z., Wang, C., Mao, D., Zhang, Y., 2019. A new vegetation index to detect periodically submerged mangrove forest using single-tide Sentinel-2 imagery. Remote Sens. 11 (17), 2043.

Jamaluddin, I., Chen, Y.N., Ridha, S.M., Mahyatar, P., Ayudyanti, A.G., 2022. Two decades mangroves loss monitoring using random forest and landsat data in east luwu, Indonesia (2000-2020). Geomatics 2 (3), 282–296.

Jiang, Y.F., Li, J., Xin, R.R., Li, Y., 2022. Spatial-temporal dynamics of coastal aquaculture ponds and its impacts on mangrove ecosystems. Chinese Journal of Plant Ecology 46 (10), 1268.

Jiang, J., Chen, Z., Sun, K., Chen, Y., Mu, M., Sun, Q., Zeng, S., 2024. Monitoring 36-year water clarity dynamics in turbid waters of the Pearl River Estuary, China, using Landsat data. Ecol. Inform. 81, 102600.

Jia, M., Wang, Z., Zhang, Y., Ren, C., Song, K., 2014. Landsat-based estimation of mangrove forest loss and restoration in Guangxi province, China, influenced by human and natural factors. IEEE J. Sel. Top. Appl. Earth Obs. Rem. Sens. 8 (1), 311–323.

Kuenzer, C., Bluemel, A., Gebhardt, S., Quoc, T.V., Dech, S., 2011. Remote sensing of mangrove ecosystems: a review. Remote Sens. 3, 878–928.

Kirwan, M.L., Megonigal, J.P., 2013. Tidal wetland stability in the face of human impacts and sea-level rise. Nature 504 (7478), 53–60.

Krauss, K.W., McKee, K.L., Lovelock, C.E., Cahoon, D.R., Saintilan, N., Reef, R., Chen, L., 2014. How mangrove forests adjust to rising sea level. New Phytol. 202 (1), 19–34.

Katlane, R., Nechad, B., Ruddick, K., Zargouni, F., 2013. Optical remote sensing of turbidity and total suspended matter in the Gulf of Gabes. Arabian J. Geosci. 6, 1527–1535.

Long, C., Dai, Z., Mei, X., Liang, X., Zhang, X., Xi, Y., Wang, R., Nguyen, A.B., Van, M.V., Cheng, J., 2025. Machine learning-based detection of dynamic changes in mangrove forest, Beilun Estuary. Ocean Coast. Manag. 266, 107696.

Long, C., Dai, Z., Wang, R., Lou, Y., Zhou, X., Li, S., Nie, Y., 2022. Dynamic changes in mangroves of the largest delta in northern Beibu Gulf, China: reasons and causes. For. Ecol. Manage. 504 (15), 119855.

Long, C., Dai, Z., Zhou, X., Mei, X., Mai Van, C., 2021. Mapping mangrove forests in the Red River Delta, Vietnam. For. Ecol. Manag. 483.

Long, H., Qu, Y., 2018. Land use transitions and land management: a mutual feedback perspective. Land Use Policy 74, 111–120.

Luo, Z., Ying, Z., 1992. The Harbours in South China. Sun Yat-sen University Press, Guangzhou (in Chinese).

Lovelock, C.E., Cahoon, D.R., Friess, D.A., Guntenspergen, G.R., Krauss, K.W., Reef, R., Rogers, K., Saunders, M.L., Sidik, F., Swales, A., Saintilan, N., Thuyen, L.X., Triet, T., 2015. The vulnerability of Indo-Pacific mangrove forests to sea-level rise. Nature 526 (7574), 559–563.

López, L., Cellone, F., 2022. SfM-MVS and GIS analysis of shoreline changes in a coastal wetland, Parque Costero del Sur biosphere reserve, Argentina. Geocarto Int. 37 (26), 11134–11150.

Li, W., Dai, Z., Mei, X., Liu, X., 2026. Seaward dynamic changes in mangrove forest over a tide-dominated estuary between 1986 and 2023. For. Ecol. Manag. 601, 123370.

Li, S., Yang, X., Huang, H., Liang, X., Wang, R., Feng, B., 2022. Variations in the suspended sediment concentration in mountain-type rivers flowing into the sea in the past 60 years-taking Nanliu River in Beibu Gulf as an example. Front. Earth Sci. 10, 913022.

Lu, J., Zhang, Y., Shi, H., Lv, X., 2023. Spatio-temporal changes and driving forces of reclamation based on remote sensing: a case study of the Guangxi Beibu Gulf. Front. Mar. Sci. 10, 1112487.

Morrissette, H.K., Baez, S.K., Beers, L., Bood, N., Martinez, N.D., Novelo, K., Andrews, G., Balan, L., Beers, C.S., Betancourt, S.A., Blanco, R., Bowden, E., Burns-Perez, V., Carcamo, M., Chevez, L., Crooks, S., Felle, i.C., Galvez, G., Garbutt, K., Gongora, R., Grijalva, E., Lefcheck, J., Mahung, A., Matti, s C., McKoy, T., McLaughlin, D., Meza, J., Pott, E., Ramirez, G., Ramnarace, V., Rash, A., Rosado, S., Santos, H., Santoya, L., Sosa, W., Ugarte, G., Viamil, J., Young, A., Young, J., Canty, S.W., 2023. Belize Blue Carbon: establishing a national carbon stock estimate for mangrove ecosystems. Sci. Total Environ. 870, 161829.

Mafi-Gholami, D., Zenner, E.K., Jaafari, A., 2020. Mangrove regional feedback to sea level rise and drought intensity at the end of the 21st century. Ecol. Indic. 110, 105972.

Maurya, K., Mahajan, S., Chaube, N., 2021. Remote sensing techniques: mapping and monitoring of mangrove ecosystem-A review. Complex Intell. Syst. 7 (6), 2797–2818.

Mondal, P., Liu, X., Fatoyinbo, T.E., Lagomasino, D., 2019. Evaluating combinations of sentinel-2 data and machine-learning algorithms for mangrove mapping in West Africa. Remote Sens. 11 (24), 2928.

Ma, C., Zhao, J., Ai, B., Sun, S., Yang, Z., 2022. Machine learning based long-term water quality in the turbid Pearl River Estuary, China. J. Geophys. Res., Oceans 127 (1) e2021JC018017.

Malik, A., Kumar, A., Piri, J., 2017. Daily suspended sediment concentration simulation using hydrological data of Pranhita River Basin, India. Comput. Electron. Agric. 138, 20–28.

Nagelkerken, I., Blaber, S.J.M., Bouillon, S., Green, P., Haywood, M., Kirton, L.G., Meynecke, J.O., Pawlik, J., Penrose, H.M., Sasekumar, A., Somerfield, P.J., 2008. The habitat function of mangroves for terrestrial and marine fauna: a review. Aquat. Bot. 89 (2), 155–185.

Nechad, B., Ruddick, K.G., Park, Y., 2010. Calibration and validation of a generic multisensor algorithm for mapping of total suspended matter in turbid waters. Remote Sens. Environ. 114 (4), 854–866.

Novoa, S., Doxaran, D., Ody, A., Vanhellemont, Q., Lafon, V., Lubac, B., Gernez, P., 2017. Atmospheric corrections and multi-conditional algorithm for multi-sensor remote sensing of suspended particulate matter in low-to-high turbidity levels coastal waters. Remote Sens. 9 (1), 61.

Nguyen, H.-H., McAlpine, C., Pullar, D., Johansen, K., Duke, N.C., 2013. The relationship of spatial-temporal changes in fringe mangrove extent and adjacent land-use: case study of Kien Giang coast, Vietnam. Ocean Coast Manag. 76, 12–22.

Nascimento Jr., W.R., Souza-Filho, P.W.M., Proisy, C., Lucas, R.M., Rosenqvist, A., 2013. Mapping changes in the largest continuous Amazonian mangrove belt using object-based classification of multisensor satellite imagery. Estuar. Coast Shelf Sci. 117, 83–93.

O'Brien, K., Stocker, J., Barrett, J., Hyde, B., 2014. Analysis of Shoreline Change in Connecticut: 100+ Years of Erosion and Accretion: Methodology and Summary Results.

Ofori, S.A., Kodikara, S.K., Jayatissa, L.P., Madarasinghe, S.K., Nijamdeen, T.M., Dahdouh-Guebas, F., 2023. What is the ecological footprint of aquaculture after 5 decades of competition between mangrove conservation and shrimp farm development? Aquat. Conserv. Mar. Freshw. Ecosyst. 33 (1), 15–28.

Pal, M., 2009. Kernel methods in remote sensing: a review. ISH Journal of Hydraulic Engineering 15 (Suppl. 1), 194–215.

Parida, B.R., Kumar, P., 2020. Mapping and dynamic analysis of mangrove forest during 2009-2019 using landsat-5 and sentinel-2 satellite data along Odisha Coast. Trop. Ecol. 61 (4), 538–549.

Pashaei, M., Kamangir, H., Starek, M.J., Tissot, P., 2020. Review and evaluation of deep learning architectures for efficient land cover mapping with UAS hyper-spatial imagery: a case study over a wetland. Remote Sens. 12 (6), 959.

Potić, I., 2015. Simple ETM+ gap fill techniques review. Environment 3 (1), 31–37.

Peterson, K.T., Sagan, V., Sidike, P., Cox, A.L., Martinez, M., 2018. Suspended sediment concentration estimation from landsat imagery along the lower missouri and middle Mississippi Rivers using an extreme learning machine. Remote Sens. 10 (10), 1503.

Qian, L.X., Li, S.F., Cui, H.S., Zhang, Y.L., 2012. Image quality evaluation of Landsat 7 ETM SLC-OFF based on a single image local regression model retrieved. Geogr. Geo-Inf. Sci. 28 (5), 21–24.

Raju, R.D., Arockiasamy, M., 2022. Coastal protection using integration of mangroves with floating barges: an innovative concept. J. Mar. Sci. Eng. 10, 612.

Richards, D.R., Friess, D.A., 2016. Rates and drivers of mangrove deforestation in Southeast Asia, 2000-2012. Proc. Natl. Acad. Sci. 113 (2), 344–349.

Rouse, J.W., Haas, R.H., Scheel, J.A., Deering, D.W., 1974. Monitoring vegetation systems in the Great Plains with ERTS. Proceedings, 3rd Earth Resource Technology Satellite (ERTS) Symposium 1, 48–62.

Rodriguez-Galiano, V.F., Ghimire, B., Rogan, J., Chica-Olmo, M., Rigol-Sanchez, J.P., 2012. An assessment of the effectiveness of a random forest classifier for land-cover classification. ISPRS J. Photogrammetry Remote Sens. 67, 93–104.

Ryu, S.O., 2003. Seasonal variation of sedimentary processes in a semi-enclosed bay: hampyong bay, Korea. Estuar. Coast Shelf Sci. 56 (3–4), 481–492.

Swales, A., Reeve, G., Cahoon, D.R., Lovelock, C.E., 2019. Landscape evolution of a fluvial sediment-rich Avicennia marina mangrove Forest: insights from seasonal and inter-annual surface-elevation dynamics. Ecosystems 1–24.

Sheykhmousa, M., Mahdianpari, M., Ghanbari, H., Mohammadimanesh, F., Ghamisi, P., Homayouni, S., 2020. Support vector machine versus random forest for remote sensing image classification: a meta-analysis and systematic review. IEEE J. Sel. Top. Appl. Earth Obs. Rem. Sens. 13, 6308–6325.

Su, J., Friess, D.A., Gasparatos, A., 2021. A meta-analysis of the ecological and economic outcomes of mangrove restoration. Nat. Commun. 12 (1), 5050.

Simard, M., Rivera-Monroy, V.H., Mancera-Pineda, J.E., Castañeda-Moya, E., Twilley, R. R., 2008. A systematic method for 3D mapping of mangrove forests based on Shuttle Radar Topography Mission elevation data, ICEsat/GLAS waveforms and field data: application to Ciénaga Grande de Santa Marta, Colombia. Remote Sens. Environ. 112 (5), 2131–2144.

Sofue, Y., Quevedo, J.M.D., Lukman, K.M., Kohsaka, R., 2025. Identifying changes in mangrove landscapes in the Philippines and Indonesia using remote sensing and community perceptions: towards ecosystem services management. Reg. Stud. Mar. Sci. 82, 104023.

Sun, Z., Jiang, W., Ling, Z., Sun, J., Zhang, Z., Huang, S., Li, Q., 2024. Rapid expansion of coastal mangrove forest in Guangxi Beibu Gulf: patterns, drivers and impacts. IEEE J. Sel. Top. Appl. Earth Obs. Rem. Sens.

Thomas, N., Lucas, R., Bunting, P., Hardy, A., Rosenqvist, A., Simard, M., 2017. Distribution and drivers of global mangrove forest change, 1996-2010. PLoS One 12 (6), e0179302.

Tinh, P.H., MacKenzie, R.A., Hung, T.D., Hanh, N.T.H., Hanh, N.H., Manh, D.Q., Ha, H. T., Tuan, M.S., 2022. Distribution and drivers of Vietnam mangrove deforestation from 1995 to 2019. Mitig. Adapt. Strategies Glob. Change 27 (4), 29.

Tao, Y.C., Ge, W.B., Liu, W.A., Pan, L.H., Qiu, G.L., Wang, X., Fan, H.Q., 2017. A survey on the spatial distribution and community types of mangroves in Guangxi based on high-resolution satellite imageries. J. Nat. Resour. 32 (9), 1602–1614.
Talaei Khoei, T., Ould Slimane, H., Kaabouch, N., 2023. Deep learning: systematic review, models, challenges, and research directions. Neural Comput. Appl. 35 (31), 23103–23124.
Torres-Córdoba, J., Valle-Levinson, A., Toro-Valencia, V.G., Cardona, Y., Paniagua-Arroyave, J.F., Aguirre-Pérez, M.C., 2025. Tidal dynamics in a quasi-rectangular semi-enclosed basin with a constriction at its flank. Estuar. Coast Shelf Sci., 109496
Vaiphasa, C., De Boer, W.F., Skidmore, A.K., Panitchart, S., Vaiphasa, T., Bamrongrugsa, N., Santitamnont, P., 2007. Impact of solid shrimp pond waste materials on mangrove growth and mortality: a case study from Pak Phanang, Thailand. Hydrobiologia 591, 47–57.
Woodroffe, C.D., Rogers, K., McKee, K.L., Lovelock, C.E., Mendelssohn, I.A., Saintilan, N., 2016. Mangrove sedimentation and response to relative sea-level rise. Ann. Rev. Mar. Sci 8 (1), 243–266.
Worthington, T.A., Ermgassen, P., Friess, D.A., Krauss, K.W., Lovelock, C.E., Thorley, J., Tingey, J., Woodroffe, C.D., Bunting, P., Cormier, N., Lagomasino, D., Lucas, R., Murray, N., Sutherland, W.J., Spalding, M., 2020. A global biophysical typology of mangroves and its relevance for ecosystem structure and deforestation. Sci. Rep. 10 (1), 14652.
Wang, D., Dai, Z., Long, C., Liang, X., Xiong, Y., Cheng, J., 2025. The serious loss of mangrove forest over the largest delta of Africa, Niger Delta: causes and reasons. Mar. Environ. Res., 107350
Wang, X., Wen, Z., Liu, G., Tao, H., Song, K., 2022. Remote estimates of total suspended matter in China's main estuaries using Landsat images and a weight random forest model. ISPRS J. Photogrammetry Remote Sens. 183, 94–110.
Wu, R., Dai, Z., Mei, X., Luo, J., Fagherazzi, S., 2025b. Profiling of mangrove forest dynamics in the Fly River delta, Papua New Guinea. Mar. Pollut. Bull. 217, 118119.
Wu, T., Pang, W., Wang, R., Huang, H., Shen, S., Huang, C., Hu, B., 2025a. Detecting dynamic changes in mangrove forests in the Dandou Sea, Beibu Gulf. Front. Earth Sci. 1–19.
Xiong, Y., Dai, Z., Long, C., Liang, X., Lou, Y., Mei, X., Nguyen, B.A., Cheng, J., 2024. Machine Learning-Based examination of recent mangrove forest changes in the western Irrawaddy River Delta, Southeast Asia. Catena 234, 107601.
Xu, H., 2006. Modification of normalised difference water index (NDWI) to enhance open water features in remotely sensed imagery. Int. J. Rem. Sens. 27 (14), 3025–3033.
Yang, J., Huang, X., 2021. 30 m annual land cover and its dynamics in China from 1990 to 2019. Earth Syst. Sci. Data Discuss. 2021, 1–29.
Yang, J., Deng, R., Ma, Y., Li, J., Guo, Y., Lei, C., 2025. An inversion model for suspended sediment concentration based on hue angle optical classification: a case Study of the coastal waters in the Guangdong-Hong Kong-Macao Greater Bay Area. Sensors 25 (6), 1728.
Yu, J., Wang, Y., 2023. Evolution of blue carbon management policies in China: review, performance and prospects. Clim. Policy 23 (2), 254–267.
Zhou, Y., Dai, Z., Liang, X., Cheng, J., 2024. Machine learning-based monitoring of mangrove ecosystem dynamics in the Indus Delta. For. Ecol. Manage. 571, 122231.
Zheng, Y., Takeuchi, W., 2020. Quantitative assessment and driving force analysis of mangrove forest changes in China from 1985 to 2018 by integrating optical and radar imagery. ISPRS Int. J. GeoInf. 9 (9), 513.
Zhou, T., Cao, B., Qiu, J., Cai, S., Ou, H., Fan, W., Yang, X., Xie, X., Bo, Y., Zhang, G., 2023. Mapping suspended sediment changes in the Western Pacific coasts. Remote Sens. 15 (21), 5192.
Zhang, Z., Jiang, W., Xiao, Z., Ling, Z., Sun, J., Song, J., Li, X., 2025. Optimal Simulation of Future Restoration and protection spatial for mangroves and assessment of disaster prevention and mitigation functions with SDG13. 1. J. Clean. Prod., 145784
Zhang, B., Xiong, W., Ma, M., Wang, M., Wang, D., Huang, X., Yu, L., Zhang, Q., Lu, H., Hong, D., Yu, F., Wang, Z., Wang, J., Li, X., Peng, G., Huang, X., 2022. Super-resolution reconstruction of a 3 arc-second global DEM dataset. Science bulletin 67 (24), 2526–2530.